Analogous piezoelectric network for multimodal vibration attenuation of a thin circular ring

Alan Luo, Boris Lossouarn, Alper Erturk

PAPER • **OPEN ACCESS**

Analogous piezoelectric network for multimodal vibration attenuation of a thin circular ring

To cite this article: Alan Luo *et al* 2023 *Smart Mater. Struct.* **32** 115024

OPEN ACCESS
IOP Publishing
Smart Materials and Structures
Smart Mater. Struct. **32** (2023) 115024 (15pp)
https://doi.org/10.1088/1361-665X/ad0139

Analogous piezoelectric network for multimodal vibration attenuation of a thin circular ring

Alan Luo[1,*], **Boris Lossouarn**[2] **and Alper Erturk**[1]

[1] G W Woodruff School of Mechanical Engineering, Georgia Institute of Technology, 771 Ferst Dr NW, Atlanta, GA 30313, United States of America
[2] Laboratoire de Mécanique des Structures et des Systémes Couplés, Conservatoire national des arts et métiers, HESAM Université, 292 rue Saint Martin, 75003 Paris, France

E-mail: luo@gatech.edu

Received 8 July 2023, revised 22 September 2023
Accepted for publication 7 October 2023
Published 16 October 2023

Abstract

Structural vibrations can be reduced by coupling to a piezoelectric electrical network that exhibits analogous modal properties of the structure. This paper considers the multimodal vibration damping of a thin circular ring using this method. The electrical network is derived by applying a finite difference model to the governing equations of motion for a segment of a thin curved beam. An electromechanical analogy is then applied to the physical constants. The resulting passive electrical network unit cell is a topology of capacitors, inductors, and transformers analogous to the dynamics of a segment of curved beam. The electrical network for a curved beam is simplified by considering an inextensional assumption and combining edge components in adjacent unit cells. The resulting simplified discrete network for a curved beam segment is assembled into a complete network for a circular ring. The electrical network for a circular ring displays modal properties similar to its mechanical analogue in both the spatial and frequency domains. As a result of the analogous modal properties across the frequency spectrum, it is shown that the network can be used to achieve multimodal vibration attenuation across a large frequency spectrum. Piezoelectric patches are used to couple the two domains. Numerical simulation of the coupled system demonstrates the effectiveness of the broadband damping effects from the analogous network. Notably, this research establishes a novelty in the field, as it not only introduces experimental validation of curved beam analogues, but also extends the investigation to encompass the coupling between a circular ring and its piezoelectric electrical network counterpart. Further experimental network optimization demonstrate the possibility of tuning the network to adapt to an imperfect mechanical ring.

Keywords: multimodal damping, vibration control, piezoelectric coupling, electrical networks, electromechanical analogy

(Some figures may appear in colour only in the online journal)

* Author to whom any correspondence should be addressed.

1. Introduction

Structures subjected to dynamic loading may produce undesirable vibrations that could cause mechanical failure or damage sensitive electrical and computer system payloads. Circular rings are important components in many mechanical systems, where the vibration control of rings have been the topic of many studies with applications to aerospace structures, circular gears [1, 2], rolling tires [3], and rotary piezoelectric motors [4].

Some of the simplest vibration control methods are purely mechanical, like the tuned mass damper [5], which can mitigate these undesired vibrations by tuning the oscillation frequency of the mass to the target mode of the structure. Hagood and von Flotow [6] proposed the mitigation of vibrations through resistive and resonant piezoelectric shunts. They demonstrated that the mechanical tuned mass damper concept may be extended to the electromechanical domain. The resonant shunt consists of a resistor and an inductor with the piezoelectric transducer acting as the capacitance in the shunt circuit. All together, these passive components create the classic electrical harmonic oscillator which has the ability to resonate at a specific frequency. By tuning the resonance frequency of the circuit to the target mode of the structure and choosing an adequate resistance value allows for a substantial vibration attenuation for a single mode. This shunt circuit can be operated in both the series and parallel resistance configurations [7]. It was also shown that the shunt could be distributed in an array around the structure to elicit a stronger coupling [8, 9].

One of the drawbacks for a single shunt circuit is that it is only capable of unimodal damping for the single target mode of the structure that the network is tuned to. Another drawback of the resonant shunt technique is that the inductance requirements may be extremely high when targeting low frequencies, in the thousands of Henrys [10]. Additional design measures need to be taken to avoid such complications such as using synthetic inductors, which can supply such high inductance through actively powered operational amplifiers [11]. Although these design measures are capable of alleviating some of the drawbacks, the system is still very sensitive to changes in inductance that depends on the long-term and environmental stability of the electronics. Any slight changes to the value of the inductance can drastically degrade the damping characteristics of the network [12]. The single mode resonant shunt is still a heavily investigated topic of research, as seen in the study conducted by Berardengo *et al* [13], where an LRLC shunt adds an additional inductor to the classic RL shunt to improve damping performance and robustness to mistuning. An alternative vibration control method uses a hybrid network, with both passive and active components, through circuits involving negative capacitance [14–17], which can be used for unimodal and multimodal damping applications. These systems have the advantage over completely passive networks in that it does not require as much precise tuning; however, active elements in the negative impedance circuit may result in stability issues.

To achieve multimodal damping, various passive techniques of connecting shunts in multiple branches have been proposed. Hollkamp proposed connecting multiple shunts parallel to each other for every target mode [11]; however, this design led to interference issues from the shunts that were not tuned to the frequency that needed to be damped. Wu [18] solved this issue by developing a current blocking circuit in series with each shunt that would cause an open circuit for all frequency modes except for the mode the shunt was tuned to, effectively increasing the tuning precision. Similarly, Behrens *et al* [19] connected current flowing circuits in series with each shunt. Yet, following these methods, single patch shunting of multiple modes has still been limited by the inability to optimize the effective electromechanical coupling coefficient to each mode, resulting in a degraded damping performance. Recently, however, studies by Raze *et al* [20] have proposed a unified tuning procedure and a comparison of the different multi-branch circuits showing that they all provide comparable performance when correctly tuned.

Adding arrays of interconnected piezoelectric transducers have been shown to increase effciency of the control from the implementation of multiple electrical resonance [21] and therefore, improving broadband damping as originally demonstrated by dell'Isola *et al* [22–24]. This solution also reduced the inductance requirements of the electrical network [25]. The concept of analogous piezoelectric network damping emerged in the early 2000s from the interest in coupling a structure to a medium with similar wave propagation properties [26]. Analogous electrical networks of mechanical structures are not a brand new concept as they were originally theorized and developed in the 1940s by MacNeal [27] for computational purposes of determining the structural responses in beams [28], plates [29], stiffened shells [30], and even entire aerospace structures [31]. Eventually, analogous electrical networks of mechanical structures were separately theorized and developed specifically for the purposes of vibration control, which had demonstrated the most optimal electromechanical coupling [32, 33]. These analogous networks were theorized for beams [34] as well as thin plates [35, 36], yet were never experimentally validated due to the complexity of the circuit architecture. Attempts of using synthetic components with operational amplifiers have been proposed in building the analogue of a beam [37], but as with active components, run into stability issues [38].

A novel unit cell was proposed with reduced components specifically for the plate [39], resulting in a redesigned and simplified electrical network. The primary novelty lies in the design of magnetic components, which enabled the implementation of fully passive analogous networks. Further numerical and experimental validation using this method was confirmed for rods [40], beams [41], plates [39, 42, 43], and most recently curved beams [44]. The addition of curvature in a structure is reflected in the added complexity in the equations of motion due to the coupling between the circumferential displacements and transverse displacements,

and thus, complicating the topology of the electrical network. The networks were tested through modal analysis to observe the electrical structure-like mode shapes. The electrical network can then be coupled to a mechanical structure using piezoelectric patches for vibration damping applications. As a result of the matching mode shapes between the electrical and mechanical domains, the network acts as a fully passive multimodal vibration absorber. Coarse arrays of piezoelectric transducers, altered boundary conditions, and local defects were introduced to the structure, yet the analogous network still produced effective multimodal damping [43].

Currently, methods for vibration control of circular structures include active H_∞ methods for cylindrical shells using piezoelectric actuators [45]. Another vibration control method for cylindrical shells utilizes arrays of passively shunted piezoelectric rings to act as sources of impedance mismatch [46]. Several other control methods using piezoelectric actuators exists for curved structures, but these methods are all considered active vibration control methods [47–49]. Piezoelectric shunts have also been applied to flat circular periodic structures like bladed disks [50, 51] using passive shunts and using semi-passive RL shunts [52, 53]. Solutions using tuned vibration absorbers have also been explored for circular rings [54]. However, no vibration control methods for circular symmetric structures that involve coupling to a fully passive electrical network with analogous modal properties have been identified as of this writing.

In this study, we extend the concept of vibration damping by an analogous electrical network to thin circular rings. In section 2, the electrical network is derived by applying a finite difference model to the governing equations of motion for a segment of a thin curved beam and applying an electromechanical analogy to the physical constants as well as the internal forces and moments. The resulting discrete network unit cell for a curved beam segment can be assembled into a complete network for a circular ring by forming a loop between the first and last unit cells. An inextensional neutral axis assumption is applied to the equations of motions of the curved beam network in order to simplify the topology of the electrical network. In section 3, a numerical simulation demonstrates that the electrical network for a circular ring displays modal properties similar to its mechanical analogue in both the spatial and frequency domain. By increasing the number of discrete unit cells in the network, it is theoretically possible to replicate the entire frequency spectrum of the ring in the electrical domain. The ring and the electrical network are coupled using piezoelectric patches, which act as capacitive elements in the network. Numerical frequency response simulations of a ring coupled to the analogous network using optimal dissipative components demonstrate the validity and effectiveness of the vibration damping theory. In the final section, experimental results verify the simulation results. Although the experimental structure was not a perfect ring, we show that numerical optimization of the network properties could still adapt to an imperfect mechanical structure.

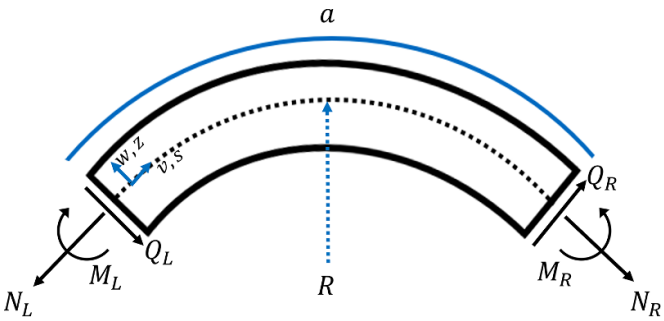

Figure 1. Continuous curved beam segment.

2. Analogous electrical network of a curved beam

2.1. Extensional equations of motion

The equations of motion for an extensional thin curved beam of density ρ, width b, thickness h, cross sectional area $S = bh$, and radius of curvature R, can be obtained using the classical theory by neglecting shear distortion and rotary inertia as established in the literature [55]. After summing the internal moments and forces of an infinitesimal segment of a curved beam shown in figure 1, the governing equations of motions are given by:

$$\frac{\partial N}{\partial s} + \frac{Q}{R} = \rho S \frac{\partial^2 v}{\partial t^2}, \qquad \frac{\partial Q}{\partial s} - \frac{N}{R} = \rho S \frac{\partial^2 w}{\partial t^2}, \tag{1}$$

where N is the normal force in the beam and Q is the shear force in the beam. The term w is the displacement in the transverse direction, denoted by the coordinate z, and the term v is the displacement in the circumferential direction, denoted by the coordinate s. Following Euler–Bernoulli beam theory, the shear force can be related to the bending moment M. Shear deformations can also be treated as negligible, so the slope of the beam θ is directly related to the displacements. Furthermore, the normal force N and the bending moment M can also be related to the displacements. With all of these assumptions, the internal forces, moments, and kinematic relationships can be rewritten as first order state equations given by:

$$\begin{aligned} Q &= -\frac{\partial M}{\partial s}, & \theta &= \frac{\partial w}{\partial s} - \frac{v}{R}, \\ M &= EI\frac{\partial \theta}{\partial s}, & N &= ES\left(\frac{\partial v}{\partial s} + \frac{w}{R}\right). \end{aligned} \tag{2}$$

where E is Young's modulus and I is the second moment of area, which for a rectangular cross-section is given by $I = \frac{1}{12}bh^3$.

2.2. Inextensional equations of motion and network simplifications

For in-plane vibrations of thin circular beams or rings, the theory of inextension can adequately determine properties of the structure vibrating at low frequencies, as derived by Lang [56]. The inextensional equations of a thin curved beam assume that the extension of the neutral axis of the ring is negligible compared to the bending deformation. The assumption relates the radial displacement and the tangential slope as $w = -R\frac{\partial v}{\partial s}$, which reduces the normal force N in equation (2) to 0, leaving the first order equations:

$$Q = -\frac{\partial M}{\partial s}, \quad M = EI\frac{\partial \theta}{\partial s}, \quad \theta = \frac{\partial w}{\partial s} - \frac{v}{R}. \tag{3}$$

Applying a finite difference scheme and an electromechanical analogy to the equations of motion [44], the discretized set of analogous electrical equations can be given as:

$$\begin{aligned}
-\frac{L}{2}\omega^2 q_{v_L} &= V_{v_L} - V_{v_I} - \frac{\hat{a}}{2\hat{R}} V_{w_L},\\
-\frac{L}{2}\omega^2 q_{v_R} &= V_{v_I} - V_{v_R} - \frac{\hat{a}}{2\hat{R}} V_{w_R},\\
-L\omega^2 q_{w_I} &= V_{w_L} - V_{w_R} + \frac{\hat{a}}{\hat{R}} V_{v_I},\\
\frac{\hat{a}}{2} V_{w_L} &= V_{\theta_L} - V_{\theta_I},\\
\frac{\hat{a}}{2} V_{w_R} &= V_{\theta_I} - V_{\theta_R},\\
C_\theta V_{\theta_I} &= q_{\theta_L} - q_{\theta_R},\\
\frac{\hat{a}}{2} q_{\theta_L} &= q_{w_I} - q_{w_L} - \frac{\hat{a}}{2\hat{R}} q_{v_L},\\
\frac{\hat{a}}{2} q_{\theta_R} &= q_{w_R} - q_{w_I} - \frac{\hat{a}}{2\hat{R}} q_{v_R},
\end{aligned} \tag{4}$$

where $\hat{a}$ is the electrical equivalent of the curved length of the unit cell, a, in the finite difference scheme. The inductance L is the electrical analogue of the mass of the unit cell, which replaces the mechanical term ρSa. Likewise, the capacitance C_θ is the electrical analogue of the bending stiffness in the unit cell, replacing the mechanical term a/EI. The corresponding analogous network for an inextensional ring can be shown in figure 2(a). This network is equivalent to the network derived by Darleux *et al* [44], but with one less capacitor due to the inextensional ring approximation.

The network may be further simplified by considering, that when assembled, the edge transformers may be combined to form a single transformer with twice the transformer ratio [41]. Furthermore, the two $L/2$ inductors can be combined into a single L inductor. Although combining the inductors is not analytically equivalent, it is a good approximation with sufficient number of unit cells. The resulting simplified network is shown in figure 2(b).

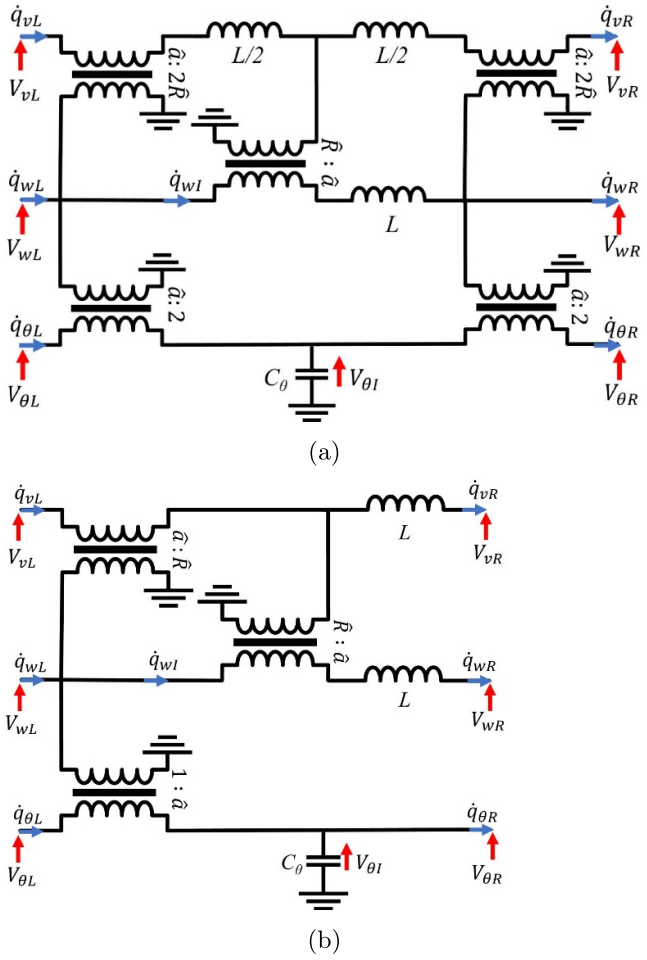

Figure 2. (a) Inextensional electrical unit cell. (b) Simplified electrical unit cell.

2.3. Spatial and frequency coherence

In order to ensure that the electrical modes correspond to the same mechanical modes, spatial and frequency conditions must be applied to determine the correct electrical constants. Spatial coherence refers to the likeness of the physical shapes of the mechanical modes to the physical shapes of the electrical modes. This not only includes ensuring adequate discretization so that the desired mode shapes may be accurately represented, but also account for the correct analogous boundary conditions in the electrical domain. Without enough unit cells in the electrical network, spatial modes may be aliased and not representative of the actual mode shapes of the ring. Spatial coherence can be assured by adhering to the criteria previously described in [40] as

$$\frac{n_{\text{element}}}{N_{\max}} \geqslant 10, \tag{5}$$

which means that the number of unit cells in the system (n_{element}) has to be ten times or greater than the maximum number of wavelengths ($N_{\max}$) in the frequency range. This ratio ensures the electrical analogue is sufficiently discretized to approximate the behavior of a continuous structure. This value

is determined from the convergence studies of the electrical network. The criteria can be used to decide on the number of unit cells necessary for the design purpose. Knowing the maximum number of wavelengths desired to be damped allows the number of electrical unit cells to be determined [44]. Furthermore, it is noted that for circular symmetrical structures, modes come in pairs with an angular shift. Therefore, there is not a singular optimal location to place a piezoelectric patch.

Frequency coherence ensures that the natural frequencies for the electrical network matches the natural frequencies of the mechanical ring which requires that the two domains have similar wave propagation properties and boundary conditions. Although applying a strict electromechanical analogy between the two domains is a possibility of ensuring frequency coherence, it is not necessary or ideal as it constrains the degree of freedom in network tuning. Instead, the frequency coherence is derived by equating the mechanical and electrical transfer matrices as shown by Darleux *et al* [44]. Furthermore, the modal assurance criteria shown by Darleux *et al* [44] also demonstrates that increased number of unit cells improves the frequency coherence for more modes. For the frequency coherence of a curved beam element, the conditions are given as:

$$\frac{a}{R} = \frac{\hat{a}}{\hat{R}}, \qquad \frac{K_\theta}{a^2 m} = \frac{1}{\hat{a}^2 L C_\theta}. \tag{6}$$

In the end, the process for deriving the analogous electrical network can be summarized by the schematic in figure 3.

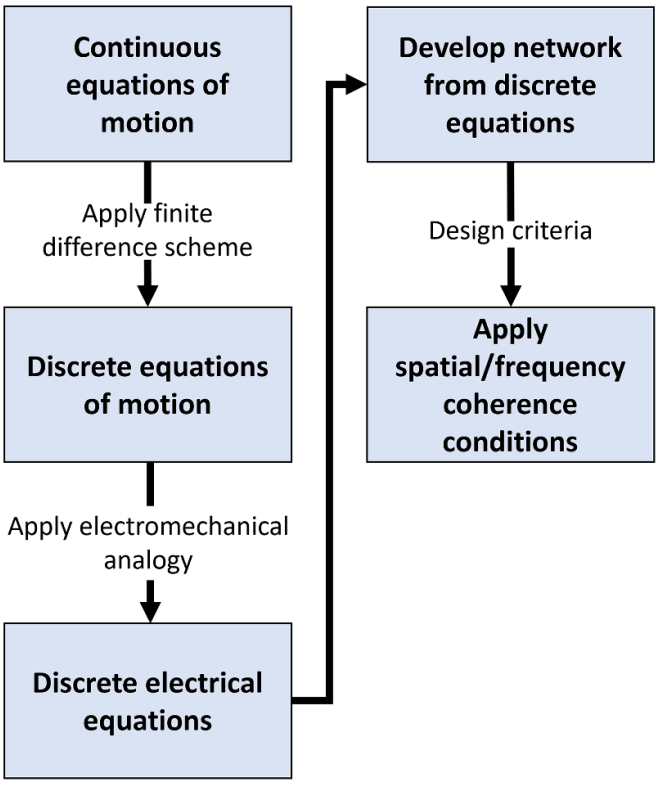

Figure 3. Network derivation process.

3. Numerical analysis

3.1. Electrical network validation

The first three in-plane circumferential bending modes are simulated for an aluminum ring with free boundary conditions of radius $R = 200$ mm, width $b = 40$ mm, and thickness $h = 5$ mm in COMSOL Multiphysics. The ring is formed from a sheet of aluminum 6061 with Poisson's ratio of 0.33, Young's Modulus of 69 GPa, and density of 2700 kg m^{-4}.

The simplified electrical network is tested using a unit cell count of $n = 100$. Since the electrical network is only representative of the circumferential bending equations, any out-of-plane twist-bending modes are not reflected in the electrical eigenvalues. For large number of unit cells, the convergence of the network is very close to the mechanical modes. The resulting eigenvalues are shown in table 1. The electrical eigenvalues are within 2% of the corresponding numerical mechanical eigenfrequencies and analytical mechanical eigenfrequencies [57], which can be given as

$$f = \frac{1}{2\pi}\sqrt{\frac{EI}{\rho S R^2}\frac{m^6 - 2m^4 + m^2}{m^2 + 1}}, \tag{7}$$

Table 1. Comparison of the natural frequencies of the electrical network using $n = 100$ unit cells to the numerical mechanical natural frequencies and analytical mechanical natural frequencies.

Analytical mechanical	Numerical mechanical	Electrical network
77.90 Hz	78.19 Hz	77.51 Hz
220.34 Hz	221.29 Hz	218.89 Hz
422.48 Hz	424.65 Hz	418.74 Hz

where m corresponds to the mode numbers. The correlation at higher modes gradually drifts apart due to the finite difference approximation and finite number of unit cells. At higher unit cell counts, it is possible to improve the correlation at higher modes [44].

From the numerical simulations, it is possible to extract the electrical currents across each inductor on the w line to construct a spatial representation of the electrical mode shapes, as shown in figure 4(a). Through the direct electromechanical analogy, the current through each inductor is equivalent to the transverse velocity of the ring at each discrete segment. Like the modes of the mechanical ring, each natural frequency has a pair of modes. Comparing the spatial visualization of the electrical mode shapes to the circumferential mechanical bending modes shown in figure 4(b), we can confirm good spatial coherence between the two domains.

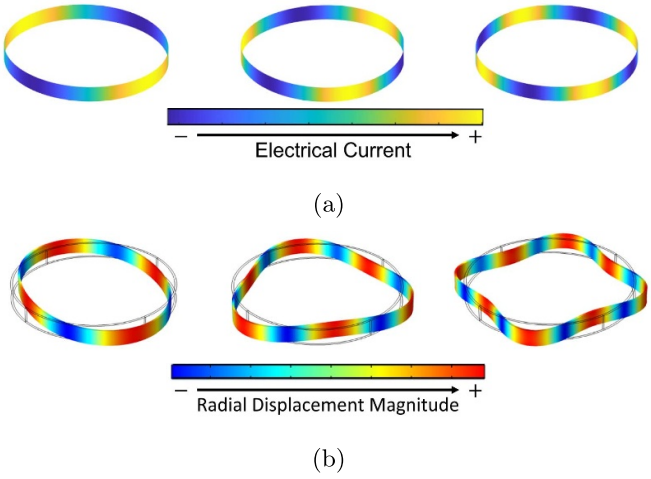

Figure 4. (a) Electrical mode shapes for a network of 100 unit cells. (b) Mechanical bending mode shapes of the circular ring.

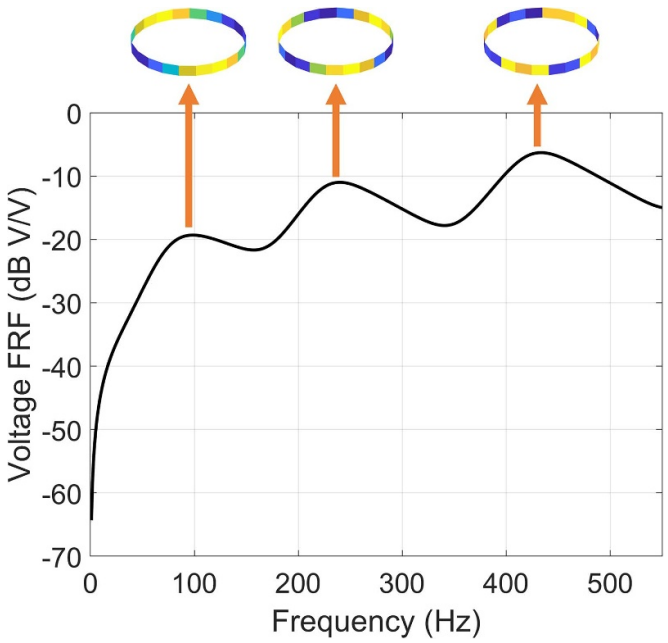

Figure 5. Electrical frequency response function of a 21 unit cell network (——), with operational mode shapes shown for each corresponding resonance.

To validate the network frequency response, an equivalent voltage excitation must be placed in between the unit cell to simulate a mechanical excitation. The equivalent voltage excitation should be placed on the transverse vibration voltage line, V_w. In the electrical network, the measurement point is the voltage across the inductor of the unit cell where the excitation voltage is applied. This measurement is equivalent to the direct drive measurement in a mechanical structure, where the acceleration of the point is measured where the excitation force is applied. Figure 5 shows the voltage frequency response of a 21 unit cell electrical network. Around the resonance frequencies, each spatial representation of the electrical current shows an operational mode shape that is similar to the corresponding mechanical mode shape, which definitively validates the analogy.

Table 2. Values of components used in the electrical unit cell.

Electrical component	Value
Capacitor (C_θ)	36 nF
Inductor (L)	418.7 mH
Transformer ($\hat{a} : \hat{R}$)	0.2992
Transformer ($\hat{a} : 1$)	4
Resistor (R)	1.56 kΩ

3.2. Modeling and simulation of the coupled system

In terms of the piezoelectric elements, PI DuraAct Patch Transducers P-876.A15 are used to couple the electrical network to the ring. The piezoelectric material in this encapsulated patch is PIC255. The full dimensions of the patch are 61 mm by 35 mm; however, the active material within the patch only measures 50 mm by 30 mm. Therefore, when modeling the patch, we consider the complete dimension of the patch in order to determine the theoretical maximum number of patches that will fit on the ring. Yet, only the dimensions of the active material is actually used to model the patch in order to accurately account for the piezoelectric effect of the patch.

Following the method used by Pernod *et al* [58], the encapsulated patch is modeled in two layers: the Kapton-glue soft layer, with thickness of 0.35 mm, and the PIC255 active layer, with thickness of 0.50 mm. By integrating the surface charge across a piezoelectric patch from a 1 V input voltage, it was observed that patch capacitance falls closer to 36 nF compared to the free capacitance at 45 nF. Furthermore, the $\hat{a} : 1$ transformer ratio is chosen to be 4:1 which comes from previously used components [39]. Using the fixed patch capacitance value and the fixed $\hat{a} : 1$ transformer ratio, the other electrical constants such as the inductance and the $\hat{a} : \hat{R}$ transformer ratio are derived from the frequency coherence conditions in equation (6). Resistors can be placed in series with the 1:4 transformers as dissipative components according to Porfiri *et al* [34] and Lossouarn *et al* [59] following

$$R_T = k_c \hat{a} \sqrt{2L/C} \tag{8}$$

where k_c is the coupling factor. Although this formulation was intended for use in thin simply supported beams, we opt to use it as a baseline approximation. The values of the electrical components are shown in table 2. We note that further manual tuning may be performed depending on application requirements.

A theoretical maximum of 21 piezoelectric patches are attached to the exterior surface of a 200 mm radius ring in the COMSOL model. The model of the ring does not consider mechanical damping. The electromechanical coupling factor, related to the conversion rate between electrical energy and

Table 3. Electromechanical coupling factors for the first six modes of the circular ring.

Mode	Coupling factors k_c
$N = 2$	12.73% and 13.04%
$N = 3$	12.80% and 13.09%
$N = 4$	12.82% and 13.15%

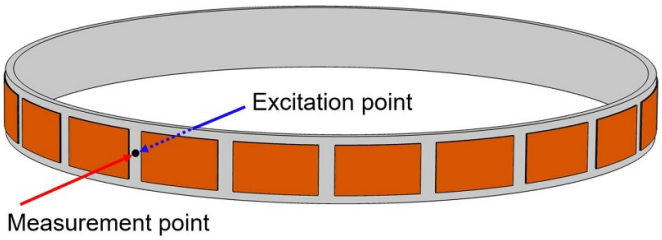

Figure 6. COMSOL Model of the ring with 21 piezoelectric patches. The drive point measurement to obtain the frequency response is indicated on the figure. The patches replace the capacitor C_θ in the network.

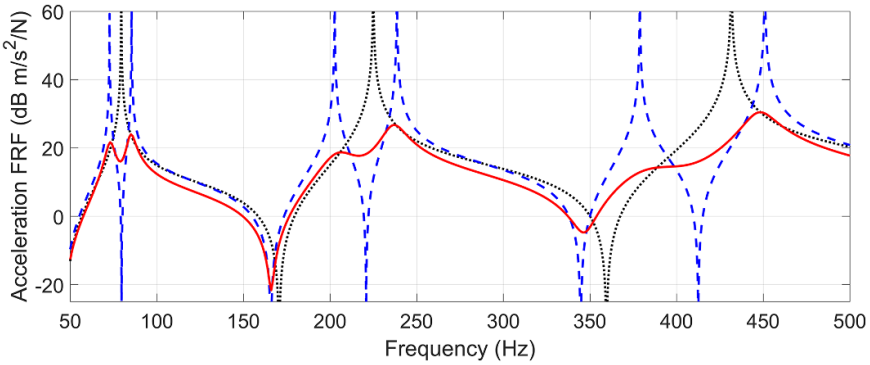

Figure 7. Frequency response functions of the ring coupled to its analogous network in open circuit (·····), with a non-dissipative electrical network (- - -), and with an optimal dissipative electrical network (——).

mechanical energy, of the piezoelectric patches is given for each mode by

$$k_c = \sqrt{\frac{\omega_{OC}^2 - \omega_{SC}^2}{\omega_{SC}^2}}, \tag{9}$$

where ω_{OC} is the open circuit frequency and ω_{SC} is the short circuit frequency of the piezoelectric ring [60]. The electromechanical coupling factors of the ring for the first six circumferential bending modes are shown in table 3. Since the addition of the patches does not strongly break the rotational symmetry, each mode exists in pairs for this circular structure. For each mode of N wavelengths, there are two separate but relatively close coupling factors.

The frequency response is measured using a direct drive method, where the measurement point coincides with the excitation point, as shown in figure 6. The coincident measurement and excitation point is chosen to be directly on the centerline axis of the ring in order to avoid any excitation of the twisting modes of the structure, which cannot be controlled by this electrical network.

A frequency response function is shown for the coupled system in figure 7. Recall that mechanical damping is not considered in the material properties for the simulation. The first three resonances are shown in the considered frequency range of the plot. For comparison, the open circuit response is shown together with the coupled responses, with a non-dissipative network and with a dissipative network. Furthermore, in figure 8, two other non-optimal dissipative networks are shown as comparison, one with 4 times the resistance and the other with 0.25 the resistance.

For a 21 unit cell network, according to the spatial coherence wavelength criteria in equation (5), only the first pair ring mode, with 2 wavelengths, can be ideally tuned. For a well tuned mode, the two local maxima on the frequency response function should have approximately the same amplitude, which is observed for the first mode ($N = 2$). At the next two higher modes ($N = 3, 4$), this is not observed, indicating that a 21 unit cells network is not enough to perfectly optimize the second and third mode, which have three and four wavelengths, respectively. Following the spatial coherence wavelength criteria previously discussed in equation (5), the electrical network should have a minimum of 40 unit cells in order to ensure that all three electromechanical mode pairs are tuned correctly. Nevertheless, using a 21 unit cell network, which considers the real dimensions of piezoelectric patches, still demonstrates strong coupling and vibration attenuation.

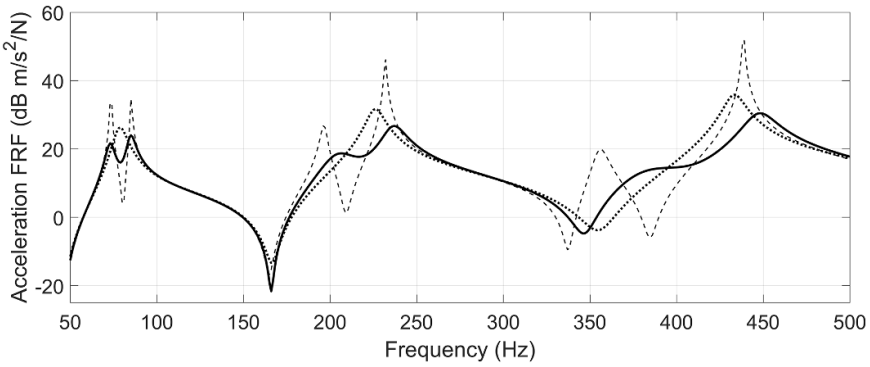

Figure 8. Frequency response functions of the ring coupled to its analogous network in with an optimal dissipative electrical network (——), with a dissipative electrical network using 4 times the optimal resistance (·····), and with a dissipative electrical network using 0.25 times the optimal resistance (- - -).

Table 4. Difference in natural frequencies between the finite element model circular ring and the experimental ring.

Numerical	Experimental	Difference
78.76 Hz	72.68 Hz	7.73%
223.45 Hz	208.60 Hz	6.64%
429.84 Hz	391.64 Hz	8.89%

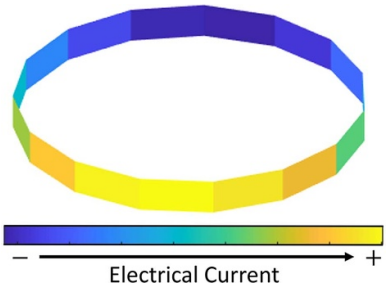

Figure 9. $N = 1$ single wavelength mode for a circular electrical network.

4. Experimental analysis

4.1. Differences between experimental setup and theoretical model

The experiment has two consequential deviations from the numerical analysis completed in the previous sections. First, the ring was not manufactured to tight tolerances, leading to a more elliptical shape, where the major axis is approximately 20 mm longer than the minor axis. Therefore, the natural frequencies of the ellipse are not exactly predictable from the governing equations of motions of a ring. A series of impulse hammer tests were conducted to measure the frequency response of the experimental mechanical structure. The accelerometer measurement is taken from the same point as the excitation of the hammer, as depicted in the setup shown in figure 6. Again, the drive point is performed on the neutral axis of the ring to avoid the excitation of the twisting modes that are not considered in the present study. The differences in the natural frequencies of the rings with patches is shown in table 4. This complication in the structure indicates that the theoretical electrical network will not provide the exact frequency coherence conditions for the ellipse.

Secondly, the realization of the electrical network requires components that are not standard and readily available. The transformers used in the experiment were developed for a previous study on multimodal plate damping by an analogous network [43, 61] and were designed to fit on a circuit board while maximizing the magnetizing inductance and minimizing the internal resistances for a specific application. As a result, the available transformers do not match the required ratio from the theory of circular rings, which is one of the frequency coherence conditions shown in equation (6).

Normally, the network would be tuned to meet frequency coherence criteria of the ring by first assigning a transformer ratio, e.g. $\hat{a} = 4$, and subsequently calculating the main tuning parameter, the inductance L, from the frequency coherence relationships shown in equation (6). However, in the experimental implementation of this electrical network, the choice in circuit components are limited by availability of the transformers. The available transformers that are used in the unit cells are preset to operate in three ratios: 1:4, 1:2, and 1:1 [43]. As a result, all of the transformers $\hat{a}:\hat{R}$ in the unit cell will use a fixed ratio of $\hat{a}:\hat{R} =$ 1:2, instead of using their theoretical value.

Because the transformer ratio $\hat{a}:\hat{R}$ is directly related to the curvature of the ring, fixing the value to 1:2 ultimately breaks the electromechanical analogy by causing a $N = 1$ (single wavelength) mode to increase to a non-zero value. In the ring, the $N = 1$ mode can be represented as figure 9. As seen in figure 10, at the theoretical transformer ratio $\hat{a}:\hat{R} =$ 0.418, the $N = 1$ mode corresponds to a rigid body motion since the transformer ratio adequately accounts for the curvature of the beam; however, as the transformer ratio increases to 1:2, the circular analogy is broken and the $N = 1$ mode becomes more prominent with higher frequencies. In any case, at the transformer ratio $\hat{a}:\hat{R} =$ 1:2, the

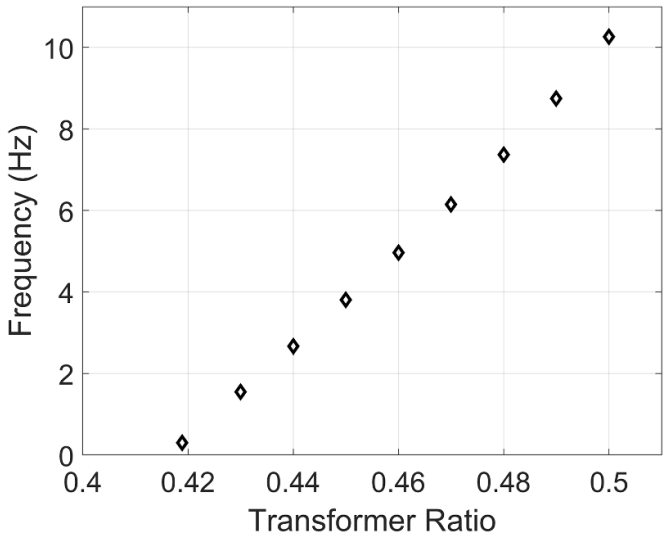

Figure 10. Frequencies of the undesired $N = 1$ (single wavelength) mode of a ring at varying $\hat{a}:\hat{R}$ transformer ratios. This plot considers a ring of 15 unit cells. The inductance is optimized for every different transformer ratio.

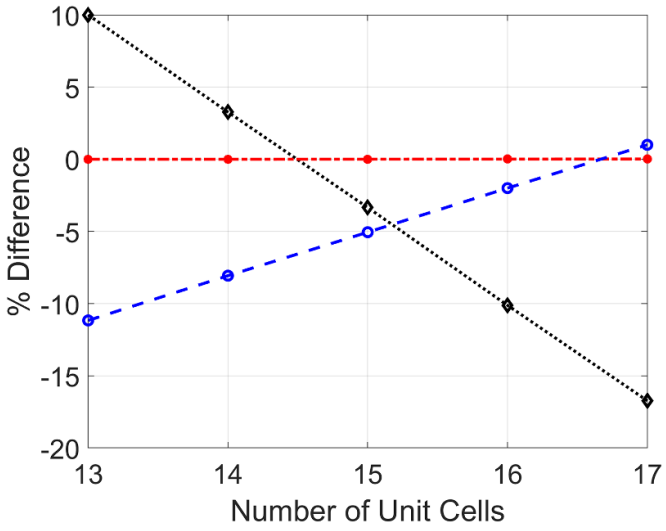

Figure 11. Optimization of the number of unit cells in the electrical network. The resulting percent difference of the electrical frequency from its analogous mechanical frequency is plotted against the number of unit cells for the first mode (◇), second mode (●), and third mode (○).

$N = 1$ is sufficiently far away from the $N = 2$ ring mode, which is the first mode that the analogy is concerned with damping.

As a result of the differences between the theoretical model and experimental setup, it is necessary to numerically optimize the electrical network to adapt to these differences from theory.

4.2. Tuning and optimizing the electrical network

The tuning of the network inductance focuses on the frequency coherence of the first three modes of the ring to account for both the fixed $\hat{a}$:$\hat{R}$ ratio as well as the elliptical shape of the experimental ring. Maximizing the quantity of unit cells on the structure no longer provides the most optimal frequency coherence due to the complications of the geometry and the fixed transformer ratio. Instead, the optimal number of electrical unit cells are computed by running an inductance optimization analysis for varying the number of unit cells, with the second mode as the main target mode of the cost function. The number of unit cell is identified from the lowest total error from the experimental mechanical ring modes. At this stage of the experiment, the parasitic elements of the transformers, like the magnetizing inductance and primary winding capacitance are not considered. These effects could be used to improve the transformer model and thus the frequency estimation [62].

In figure 11, the percent difference between the electrical frequencies and its analogous mechanical frequencies is shown against the number of unit cells. The main cause of the deviation of modes 1 and 3 at higher unit cell numbers is again due to fixing the $\hat{a}$:$\hat{R}$ transformer ratio to 1:2 instead of using the analytical value. As a result, a network of 15 unit cells is chosen since the total error between the mechanical and electrical modes is the lowest in this configuration. The associated three electrical modes for 15 unit cells are shown in table 5.

Table 5. First three electrical modes of the network computed with the optimized inductor ($L = 1.1$ H) compared to the experimental mechanical modes.

Mechanical modes	Electrical modes	Difference
72.68 Hz	70.246 Hz	−3.34%
208.60 Hz	208.60 Hz	0.00%
391.64 Hz	371.84 Hz	−5.05%

The capacitance in the analogous network is estimated by the measuring directly across the patches on the ring from 20 Hz to 500 Hz using an impedance meter. All 15 patches are measured and compared with the numerical model. Since the patch capacitance is a function of frequency, it is necessary to determine the average capacitance across a range of frequencies in the design criteria. In the numerical model, the patch capacitance may be calculated by applying a 1 V electrical potential to the patch while sweeping across a range of frequencies. Then, the surface charge density is determined by integrating across surface of the patch. The resulting charge density is equivalent to the patch capacitance due to the unit voltage. The average experimental capacitance of all 15 patches is approximately 34 nF as compared to the 36 nF estimated in the simulation, as shown in figure 12. This difference can be attributed to: a slight overestimation of the thickness of the Kapton-glue layer, or an approximate permittivity of the piezoelectric material. The 34 nF capacitance

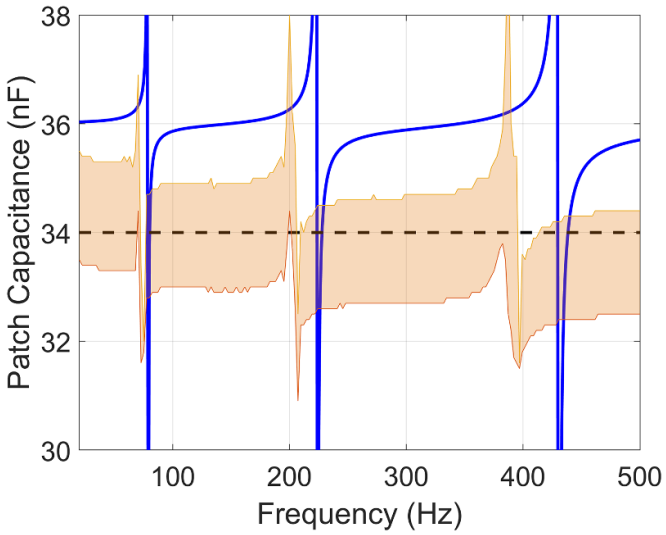

Figure 12. Patch capacitance as a function of frequency. The patch capacitance obtained from admittance computation in COMSOL (——) is approximately 36 nF. The range of capacitance for all 15 experimental piezoelectric patches is highlighted (■). The average experimental patch capacitance is approximately 34 nF (- - -).

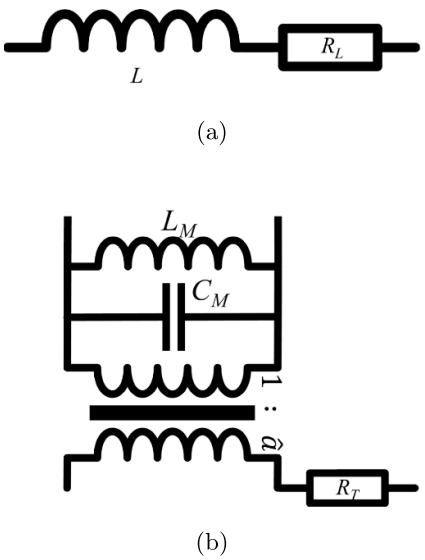

Figure 13. (a) Inductor model with a resistor connected in series. (b) Transformer model with primary winding capacitance, magnetizing inductance, and winding resistance.

value is then used to optimize the experimental network inductance.

4.3. Validating voltage frequency response of the network

When modeling realistic inductors and transformers, it is necessary to take the internal resistances, magnetizing inductance, and capacitative effects into account. Realistic inductors are modeled with a series resistor representing the copper losses in the winding, as shown in figure 13(a). The transformer model shown in figure 13(b) includes three additional passive components: the internal resistance, the magnetizing inductance, and the primary winding capacitance. Some literature [62] often include the secondary winding capacitance and interwinding capacitance; however, in this experiment, these values are deemed low enough to remove to from the model in order to simplify the electrical network. The magnetic component values are experimentally measured and are shown in table 6. The transformer of ratio 1:2 refers to the $\hat{a} : \hat{R}$ transformer, and the transformer of ratio 1:4 refers to the $1 : \hat{a}$ transformer.

The voltage frequency response of the network is measured with a drive point measurement to stay consistent with the previous acceleration frequency response measurements. The 'w line' inductor voltage is measured at the same unit cell as the excitation voltage source. To avoid introducing an unwanted ground in the network direct voltage excitation is avoided. Instead, a 1:1 transformer is used as a buffer between the voltage source and the rest of the network in order to maintain the circuit topology and measure the correct frequency response.

Table 6. Values of realistic magnetic components. Note that all capacitance values are measured at 10 kHz (high frequency limit) and all inductance values are measured at 20 Hz (low frequency limit).

Component	Value
Inductor	$L = 1.2$ H $R_L = 64\ \Omega$
Transformer 1:2	$L_M = 16$ H $C_M = 4$ nF $R_T = 64\ \Omega$
Transformer 1:4	$L_M = 16$ H $C_M = 20$ nF $R_T = 272\ \Omega$

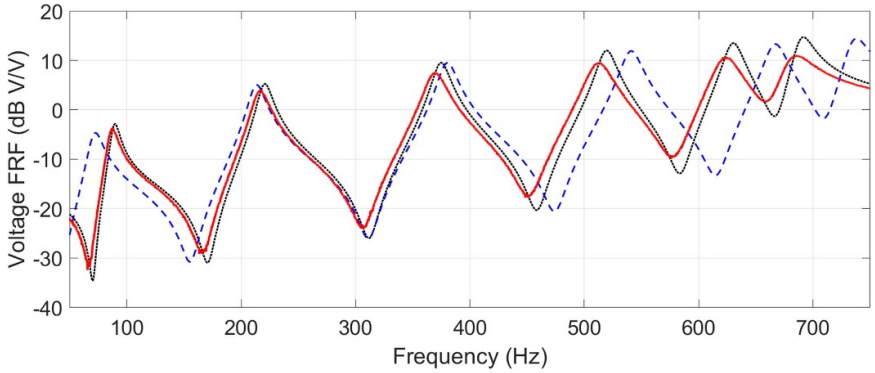

Figure 14. Voltage frequency response function of experimental network (——), numerical network without considering magnetizing inductance and primary winding capacitance (- - -), and numerical network considering magnetizing inductance and primary winding capacitance (·····).

The piezoelectric patches are replaced by capacitors that have the similar free capacitance values in order to measure the correct frequency response. The closest commercial capacitors available are 33 nF. The voltage frequency response for the analogous network is shown in figure 14 where the matching resonances and anti-resonances demonstrates a clear correlation between simulation and experiment. In an electrical network, the resonances correspond to high currents and anti-resonances correspond to low currents, analogous to the velocity in a damped mechanical structures. The incorporation of magnetizing inductance and winding capacitance into the electrical network improves the accuracy of the numerical simulations.

Although the effects of parasitic elements in the network are considered for the modeling of the voltage frequency response, we do not consider these effects for updating the tuning of the network of the coupled system because it does not lead to a strong difference with respect to the proposed experimental implementation.

4.4. Broadband damping of a ring coupled to its analogous network

The electrical network is assembled with 15 unit cells. The piezoelectric patches on the structures are connected to the capacitance node, shown in figure 15. The network consists of 30 transformers of ratio 1:2, 15 transformers of ratio 1:4, and 30 inductors of inductance 1.2 H.

A modal hammer test is conducted to measure a drive point frequency response, as previously conducted for the uncoupled ring. The resulting experimental coupled frequency response is shown in figure 16(a). A similar frequency response, shown in figure 16(b), is produced numerically using an ideal circular ring coupled to an ideal 15 unit cell network. We do not consider mechanical damping in the numerical model of the structure. Resistances in the network are modeled after the measured resistance values shown in table 6 for each component. There appears to be good correlation between the experimental and numerical results, which follow similar frequency response trends. The second mode for both frequency responses is able to achieve strong vibration attenuation with approximately 30 dB of attenuation in the experimental case. Less ideal attenuation is observed for the first and third modes, where we can see that the two peaks of the electromechanical modes are not centered symmetrically around the open-circuit mechanical mode, indicating sub-optimal tuning. Nevertheless, approximately 10 dB of vibration reduction is still achieved. This is due to an inadequate number of unit cells in the network. In comparison, we can see in the simulated 21 unit cell model in figure 7 that there is high attenuation in more modes due to more unit cells in the network and thus better multimodal tuning.

(a)

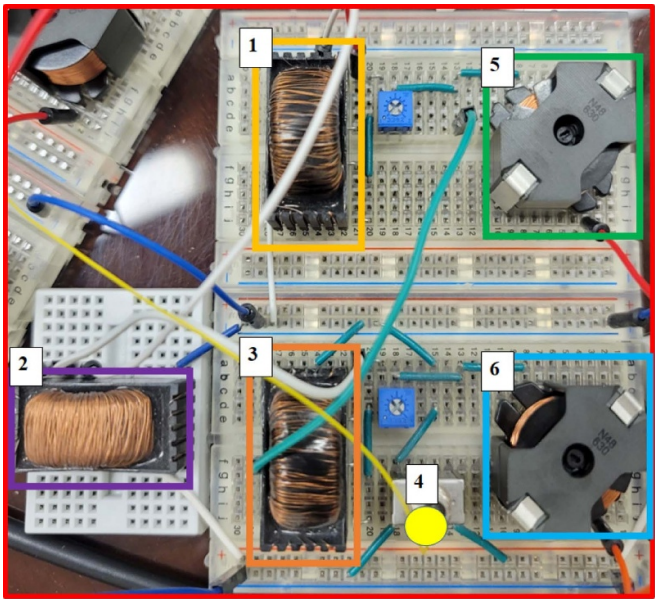

(b)

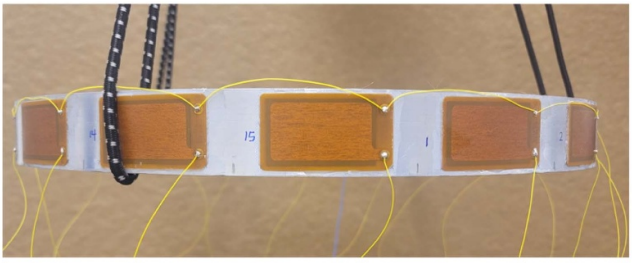

(c)

Figure 15. (a) Experimental setup of the analogous 15 unit cell electrical network for a ring. (b) Circuit setup of a single unit cell: (1) $\hat{a}:\hat{R}$ Transformer. (2) $1:\hat{a}$ Transformer. (3) $\hat{R}:\hat{a}$ Transformer. (4) Piezoelectric patch connection. (5) 'v' Inductor. (6) 'w' Inductor.
(c) Experimental aluminum ring with piezoelectric patches attached.

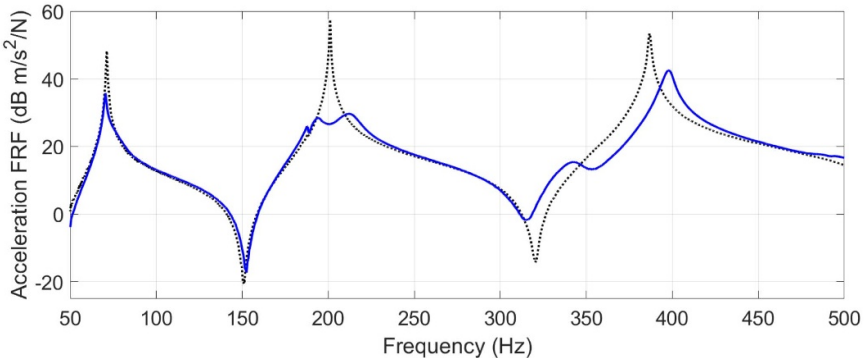

(a) Experimental frequency response.

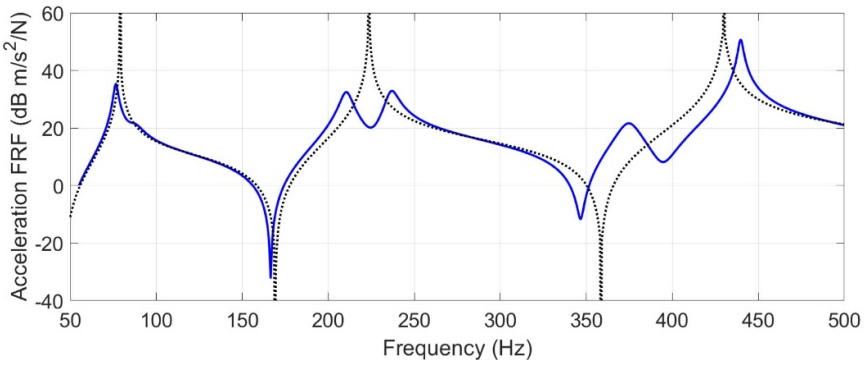

(b) Simulated frequency response.

Figure 16. Experimental and simulated frequency response functions of a thin ring coupled its analogous electrical network. Frequency response functions for a 15 unit cell ring in open circuit configuration (·····), and coupled to the analogous network (——).

Finally, the experimental setup shows more internal resistance than the numerical model despite being modeled with the same internal resistance values. This is most likely the result of the non-modeled iron losses in the magnetic components.

5. Conclusion

This study investigated the multimodal damping of a piezoelectric circular ring connected to an analogous electrical network. The analogous network was designed to exhibit the same modal properties as a mechanical ring structure. The previously derived network for a curved beam was simplified using the inextensional assumption of the neutral axis of the ring. Further simplifications involved combining adjacent transformers and inductors, effectively reducing the number of components in the electrical network. Spatial and frequency coherence was verified, which validated the analogy between the ring and the electrical network.

Numerical simulations were conducted using practical considerations, such as modeling encapsulated piezoelectric patches bonded to the curvature of the ring and optimal network resistance based on coupling factors. Significant vibration attenuation was observed when the ring was coupled to an optimally dissipative network, with close to optimal tuning observed for the first mode. Less optimal tuning occurred for the second and third modes due to the insufficient number of unit cells along the circumference of the ring, but vibration attenuation was still significant.

This study is the first to successfully demonstrate assembling a closed analogous piezoelectric network within a ring structure with experimental validation. The experimental portion of the study required additional numerical optimization due to several complications involving defects in the ring and predetermined ideal electrical components. Despite the complications, by using numerical optimization to leverage the degree of freedom we have in tuning, the inductance values were optimized in the electrical network to account for these deviations from theory. The inability of the coupled system to achieve high attenuation for all three modes is attributed to insufficient number of unit cells in the network. The experimental results showed good correlation with numerical results, both showing similar frequency response trends.

Although strong multimodal vibration attenuation of the circular ring was observed in the final implementation, improvements can be made to further optimize the damping. To enhance the setup, it is recommended to increase the number of unit cells in the ring to account for the spatial coherence conditions. Additionally, leveraging transformer ratios directly derived from analytical equations can further improve the system configuration. Notably, as the number of unit cells increases, the inductance per unit cell decreases, reducing the impact of the magnetizing inductance and the parasitic iron losses. These suggested enhancements hold

promise for improving the effectiveness of the multimodal vibration control system of axisymmetric structures from analogous piezoelectric networks.

Data availability statement

All data that support the findings of this study are included within the article (and any supplementary files).

Acknowledgments

This research was funded in part by the Chateaubriand Fellowship awarded by the Embassy of France in the United States. The fellowship opened up opportunities for collaboration and professional development. The authors also thank Frédéric Guillerm (Cnam) for the contributions to the experimental setup.

ORCID iDs

Alan Luo https://orcid.org/0000-0002-2266-4786
Boris Lossouarn https://orcid.org/0000-0001-7382-3137
Alper Erturk https://orcid.org/0000-0003-0110-5376

References

[1] Xu H and Qin D 2019 Vibration characteristics of flexible spur ring gears using different connection types *J. Low Freq. Noise Vib. Act. Control* **39** 246–57
[2] Wang S-Y and Meesap C 2018 Investigation on mesh and sideband vibrations of helical planetary ring gear using structure, excitation and deformation symmetries *Chin. J. Mech. Eng.* **31** 104
[3] Gong S 1989 *A comparison of vibrational properties of various tire ring model* 89.3.VT.2663 TU Delft
[4] Zhang P 2010 Sensors and actuators *Advanced Industrial Control Technology* ed P Zhang (William Andrew Publishing) ch 3, pp 73–116
[5] Rahimi F, Aghayari R and Samali B 2020 Application of tuned mass dampers for structural vibration control: a state-of-the-art review *Civ. Eng. J.* **6** 1622–51
[6] Hagood N W and von Flotow A 1991 Damping of structural vibrations with piezoelectric materials and passive electrical networks *J. Sound Vib.* **146** 243–68
[7] Yamada K, Matsuhisa H, Utsuno H and Sawada K 2010 Optimum tuning of series and parallel lr circuits for passive vibration suppression using piezoelectric elements *J. Sound Vib.* **329** 5036–57
[8] Spadoni A, Ruzzene M and Cunefare K 2009 Vibration and wave propagation control of plates with periodic arrays of shunted piezoelectric patches *J. Intell. Mater. Syst. Struct.* **20** 979–90
[9] Thorp O, Ruzzene M and Baz A 2001 Attenuation and localization of wave propagation in rods with periodic shunted piezoelectric patches *Smart Mater. Struct.* **10** 979–89
[10] Fleming A J, Behrens S and Moheimani S O R 2003 Reducing the inductance requirements of piezoelectric shunt damping systems *Smart Mater. Struct.* **12** 57–64
[11] Hollkamp J J 1994 Multimodal passive vibration suppression with piezoelectric materials and resonant shunts *J. Intell. Mater. Syst. Struct.* **5** 49–57
[12] Andreaus U and Porfiri M 2006 Effect of electrical uncertainties on resonant piezoelectric shunting *J. Intell. Mater. Syst. Struct.* **18** 477–85
[13] Berardengo M, Høgsberg J, Manzoni S, Vanali M, Brandt A and Godi T 2020 LRLC-shunted piezoelectric vibration absorber *J. Sound Vib.* **474** 115268
[14] Beck B S, Cunefare K A and Collet M 2013 Response-based tuning of a negative capacitance shunt for vibration control *J. Intell. Mater. Syst. Struct.* **25** 1585–95
[15] Casadei F, Beck B S, Cunefare K A and Ruzzene M 2012 Vibration control of plates through hybrid configurations of periodic piezoelectric shunts *J. Intell. Mater. Syst. Struct.* **23** 1169–77
[16] Tateo F, Collet M, Ouisse M, Ichchou M N, Cunefare K A and Abbe P 2014 Experimental characterization of a bi-dimensional array of negative capacitance piezo-patches for vibroacoustic control *J. Intell. Mater. Syst. Struct.* **26** 952–64
[17] Berardengo M, Thomas O, Giraud-Audine C and Manzoni S 2016 Improved resistive shunt by means of negative capacitance: new circuit, performances and multi-mode control *Smart Mater. Struct.* **25** 075033
[18] Wu S-Y 1998 Method for multiple mode piezoelectric shunting with single PZT transducer for vibration control *J. Intell. Mater. Syst. Struct.* **9** 991–8
[19] Behrens S, Moheimani S and Fleming A 2003 Multiple mode current flowing passive piezoelectric shunt controller *J. Sound Vib.* **266** 929–42
[20] Raze G, Dietrich J and Kerschen G 2022 Tuning and performance comparison of multiresonant piezoelectric shunts *J. Intell. Mater. Syst. Struct.* **33** 2470–91
[21] Raze G, Dietrich J, Lossouarn B and Kerschen G 2022 Shunts vs networks: tuning and comparison of centralized and decentralized piezoelectric vibration absorbers *Smart Mater. Struct.* **31** 115006
[22] dell'Isola F and Vidoli S 1998 Continuum modelling of piezo electromechanical truss beams: an application to vibration damping *Arch. Appl. Mech.* **68** 1–19
[23] Porfiri M, dell'Isola F and Santini E 2005 Modeling and design of passive electric networks interconnecting piezoelectric transducers for distributed vibration control *Int. J. Appl. Electromagn. Mech.* **21** 69–87
[24] dell'Isola F, Maurini C and Porfiri M 2004 Passive damping of beam vibrations through distributed electric networks and piezoelectric transducers: prototype design and experimental validation *Smart Mater. Struct.* **13** 299–308
[25] Maurini C, dell'Isola F and Del Vescovo D 2004 Comparison of piezoelectronic networks acting as distributed vibration absorbers *Mech. Syst. Signal Process.* **18** 1243–71
[26] Vidoli S and dell'Isola F 2000 Modal coupling in one-dimensional electromechanical structured continua *Acta Mech.* **141** 03
[27] MacNeal R H 1949 The solution of partial differential equations by means of electrical networks *PhD Thesis* California Institute of Technology (https://doi.org/10.7907/PZ04-5290)
[28] Benscoter S U and MacNeal R H 1952 Introduction to electrical-circuit analogies for beam analysis *Technical Report*
[29] Benscoter S U and MacNeal R H 1952 Equivalent-plate theory for a straight multicell wing *Technical Report*
[30] MacNeal R H 1954 Electrical analogies for stiffened shells with exible rings *Technical Report* (NACA)

[31] MacNeal R H 1962 *Electric Circuit Analogies for Elastic Structures* (*Airplane, Missle and Spacecraft Structure Series*) (Wiley Canada, Limited)

[32] Alessandroni S, dell'Isola F and Porfiri M 2002 A revival of electric analogs for vibrating mechanical systems aimed to their efficient control by PZT actuators *Int. J. Solids Struct.* **39** 5295–324

[33] dell'Isola F, Porfiri M and Vidoli S 2003 Piezo-electromechanical (PEM) structures: passive vibration control using distributed piezoelectric transducers *C. R. Mec.* **331** 69–76

[34] Porfiri M, dell'Isola F and Frattale Mascioli F M 2004 Circuit analog of a beam and its application to multimodal vibration damping, using piezoelectric transducers *Int. J. Circuit Theory Appl.* **32** 167–98

[35] Alessandroni S, Andreaus U, dell'Isola F and Porfiri M 2005 A passive electric controller for multimodal vibrations of thin plates *Comput. Struct.* **83** 1236–50

[36] Alessandroni S, Andreaus U, dell'Isola F and Porfiri M 2004 Piezo-electromechanical (PEM) kirchho-love plates *Eur. J. Mech.* A **23** 689–702

[37] Panella M, Paschero M and Mascioli F F 2005 Optimised RC-active synthesis of PEM networks *Electron. Lett.* **41** 1041–3

[38] Panella M, Paschero M and Mascioli F F 2006 Stability analysis of optimal PEM networks *Electron. Lett.* **42** 961–3

[39] Lossouarn B, Aucejo M, Deu J-F and Cunefare K A 2018 Design of a passive electrical analogue for piezoelectric damping of a plate *J. Intell. Mater. Syst. Struct.* **29** 1301–14

[40] Lossouarn B, Aucejo M and Deü J-F 2015 Multimodal coupling of periodic lattices and application to rod vibration damping with a piezoelectric network *Smart Mater. Struct.* **24** 045018

[41] Lossouarn B, Deu J-F and Aucejo M 2015 Multimodal vibration damping of a beam with a periodic array of piezoelectric patches connected to a passive electrical network *Smart Mater. Struct.* **24** 115037

[42] Lossouarn B, Deü J-F, Aucejo M and Cunefare K A 2016 Multimodal vibration damping of a plate by piezoelectric coupling to its analogous electrical network *Smart Mater. Struct.* **25** 115042

[43] Darleux R, Lossouarn B and Deü J-F 2020 Broadband vibration damping of non-periodic plates by piezoelectric coupling to their electrical analogues *Smart Mater. Struct.* **29** 02

[44] Darleux R, Lossouarn B, Giorgio I, dell'Isola F and Deü J-F 2022 Electrical analogs of curved beams and application to piezoelectric network damping *Math. Mech. Solids* **27** 578–601

[45] Tani J, Qiu J and Miura H 1995 Vibration control of a cylindrical shell using piezoelectric actuators *J. Intell. Mater. Syst. Struct.* **6** 380–8

[46] Thorp O, Ruzzene M and Baz A 2005 Attenuation of wave propagation in fluid-loaded shells with periodic shunted piezoelectric rings *Smart Mater. Struct.* **14** 594

[47] Sonti V R and Jones J D 1996 Curved piezoactuator model for active vibration control of cylindrical shells *AIAA J.* **34** 1034–40

[48] Zhai J, Shang L and Zhao G 2020 Topology optimization of piezoelectric curved shell structures with active control for reducing random vibration *Struct. Multidiscip. Optim.* **61** 1439–52

[49] Lester H C and Lefebvre S 1993 Piezoelectric actuator models for active sound and vibration control of cylinders *J. Intell. Mater. Syst. Struct.* **4** 295–306

[50] Yu H and Wang K W 2007 Piezoelectric networks for vibration suppression of mistuned bladed disks *J. Vib. Acoust.* **129** 559–66

[51] Wang K W and Tang J 2008 Adaptive structural systems with piezoelectric transducer circuitry

[52] Pohl M and Rose M 2016 Piezoelectric shunt damping of a circular saw blade with autonomous power supply for noise and vibration reduction *J. Sound Vib.* **361** 20–31

[53] Mokrani B, Bastaits R, Romanescu I, Horodinca M, Burda I and Preumont A 2018 Passive damping of rotationally periodic structures with tuned piezoelectric inductive shunt *Actuators* **7** 41

[54] Boukadia R F, Sangiuliano L, Claeys C, Ichchou M, Desmet W and Deckers E 2021 Vibration damping of flexible rotating rings using simple and double modes tuned vibration absorbers *2021 15th Int. Congress on Artificial Materials for Novel Wave Phenomena* (*Metamaterials*) pp 062–4

[55] Chidamparam P and Leissa A W 1993 Vibrations of planar curved beams, rings and arches *Appl. Mech. Rev.* **46** 467–83

[56] Lang T 1962 *Vibration of Thin Circular Rings* JPL-TR-32-261 Jet Propul. Lab. Calif. Inst. Technol.

[57] Rao S 2007 Vibration of circular rings and curved beams *Vibration of Continuous Systems* (Wiley) ch 12, pp 393–407

[58] Pernod L, Lossouarn B, Astolfi J A and Deü J-F 2021 Vibration damping of marine lifting surfaces with resonant piezoelectric shunts *J. Sound Vib.* **496** 115921

[59] Lossouarn B, Kerschen G and Deü J-F 2021 An analogue twin for piezoelectric vibration damping of multiple nonlinear resonances *J. Sound Vib.* **511** 116323

[60] American National Standards Institute, Institute of Electrical and Electronics Engineers 1988 IEEE standard on piezoelectricity *ANSI/IEEE Std 176-1987* (https://doi.org/10.1109/IEEESTD.1988.79638)

[61] Darleux R 2020 Development of analogous piezoelectric networks for the vibration damping of complex structures *PhD Thesis* (available at: www.theses.fr/2020HESAC011)

[62] Demumieux P, Aviñó O, Buttay C, Martin C, Sixdenier F, Joubert C, Ngo J, Magambo T and Löher T 2019 Design of a low-capacitance planar transformer for a 4 kW/500 kHz DAB converter